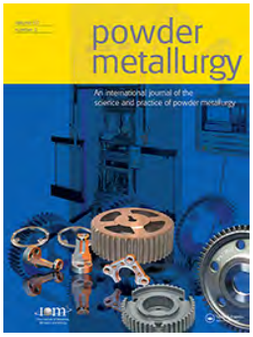

Powder Metallurgy

ISSN: 0032-5899 (Print) 1743-2901 (Online) Journal homepage: https://www.tandfonline.com/loi/ypom20

Dynamic properties of high-density low-alloy PM steels

Lin Zhang, Zhiwei Liu, Haishen Sun, Mingli Qin, Xuanhui Qu & Yuanzhi Lyu

To cite this article: Lin Zhang, Zhiwei Liu, Haishen Sun, Mingli Qin, Xuanhui Qu & Yuanzhi Lyu (2017) Dynamic properties of high-density low-alloy PM steels, Powder Metallurgy, 60:1, 56-65, DOI: 10.1080/00325899.2016.1274815

To link to this article: https://doi.org/10.1080/00325899.2016.1274815

Published online: 16 Jan 2017.

Submit your article to this journal

Article views: 122

View related articles

View Crossmark data

Citing articles: 2 View citing articles

Full Terms & Conditions of access and use can be found at
https://www.tandfonline.com/action/journalInformation?journalCode=ypom20

POWDER METALLURGY, 2017
VOL. 60, NO. 1, 56–65
http://dx.doi.org/10.1080/00325899.2016.1274815

Dynamic properties of high-density low-alloy PM steels

Lin Zhang[a], Zhiwei Liu[a], Haishen Sun[a], Mingli Qin[a], Xuanhui Qu[a] and Yuanzhi Lyu[b]

[a]Institute for Advanced Materials and Technology, University of Science and Technology Beijing, Beijing, China; [b]Laiwu Xinyi Powder Metallurgy Products Co. Ltd, Shandong, China

ABSTRACT
PM steels with density higher than 7.5 g cm^{-3} were prepared from binder-treated powder, and the effects of alloying elements and microstructure on dynamic performance were studied. Although the addition of 1.5 wt-% Cu improves the tensile strength, it impairs toughness of the alloy by the formation of low-toughness pearlite. The 0.5 wt-% Cr addition promotes the formation of Ni-rich martensite and bainite at the expense of pearlite, which is beneficial to strengthen and homogenise the microstructure. The 0.5Cr alloy exhibits improved tensile strength and fatigue strength without sacrificing impact toughness, which exhibits high potential to be used for dynamic and cyclic loading applications. The tensile strength and fatigue endurance strength under 10^7 cycles of 0.5Cr alloy achieve 1350 and 562 MPa respectively, and impact energy is as high as 21.1 J. The enhanced fatigue life is attributed to the high density, smaller pore size, rounder pores and composite-like microstructure.

ARTICLE HISTORY
Received 18 August 2016
Accepted 15 December 2016

KEYWORDS
Powder metallurgy; low-alloy steels; high density; impact toughness; fatigue properties

Introduction

Low-alloy powder metallurgy (PM) steels are used extensively in the industry and are mainly produced for automobile and mechanical parts [1,2]. Due to the presence of pores, the mechanical properties of PM steels are inferior to those of wrought counterparts, which prevent their widespread applications. The development of high-density PM steels provides the possibility of the replacement of some wrought counterparts by PM sintered steels, and a further expansion of the applications of PM sintered low-alloy steels is expected in the future [3,4]. High-density PM steels exhibit the advantages of high strength and high loading capacity, which are attractive candidates for structural components. They find numerous applications in automotive, transmission components and the other critical applications where dynamic and cyclic loading is an important consideration, such as connecting rods, transmission gears, sprockets, nozzles, cam shat pulleys, pump parts, valve seat inserts, etc [5,6]. During service conditions, these engineering components are occasionally exposed to dynamic types of loads. Dynamic properties such as impact toughness and fatigue strength are important design parameters for the selection of PM steels for numerous engineering components.

Many factors affect the dynamic properties of low-alloy PM steels, mainly including alloying compositions, density, pore shape and size, microstructure, residual stress, inclusions, etc [7,8]. It is known that porosity strongly limits the dynamic properties of PM steels due to the reduction of effective load bearing section and the presence of serious local stress and strain concentration [9]. Although porosity is effectively reduced in high-density PM steels, residual porosity still exerts pronounced influence on fatigue life and reliability of PM steels. Thus, it is of vital significance to elucidate the effect of porosity on dynamic properties of PM steels. Optimisation of alloying compositions is another important aspect in order to achieve a good combination of tensile strength and dynamic properties of high-density PM steels. Among the main added alloying elements Cu, Mo, Ni and Cr, Mo impairs the toughness of Ni-containing PM steels, while Cr and Ni improve the impact toughness and tensile strength [10,11]. The content of Cu should be optimised by the balance between the improved bonding between particles and the formation of retained austenite [12]. The effects of alloying elements on impact toughness are quite complex and still inconclusive. Microstructure also shows great influence on PM sintered steels. Up till now, there is no clear conclusion that states which microstructure is preferred in relation to dynamic performance. Moreover, the interaction between alloying composition, porosity, microstructure and dynamic property is far from being understood and established.

To develop high-strength PM steels with satisfactory tensile strength, impact toughness and fatigue strength, the effects of alloying elements and microstructure on the impact and fatigue performance of the PM sintered low-alloy steels with density higher than 7.5 g cm^{-3} were investigated. The microscopic analysis of the impact- and fatigue-fractured surfaces was carried

CONTACT Lin Zhang zhanglincsu@163.com
© 2017 Institute of Materials, Minerals and Mining Published by Taylor & Francis on behalf of the Institute

out to present the crack initiation and propagation process. This work provides useful information for the design of PM components subjected to both static and dynamic types of loads.

Experimental

Three kinds of binder-treated powder mixture with relatively high apparent density (3.05 g cm^{-3}) were designed, and the chemical compositions of these alloys are listed in Table 1. Elemental power Ni, Mo, Cu and Fe–Cr alloy powder with size of 1–3 μm were used as raw material. Figure 1 shows the SEM morphology of the binder-treated ferrous powder mixture. It is seen that fine powder Ni, Mo, Cu and Fe–Cr uniformly adhere to large iron particles.

The samples were prepared by re-compaction and re-sintering method. The first compaction was carried out to density level of 7.0 g cm^{-3}. After presintered at 800°C for 2 h in an endogas atmosphere, double compaction was carried out to obtain a density level of 7.55 g cm^{-3}. Subsequently, the samples were sintered at 1120°C for 2 h in an endogas atmosphere. The sintered samples were oil quenched at 860°C, followed by tempering at 180°C for 1 h.

The porosity measured by Archimedes method. The geometry and morphology of the of the unnotched fatigue test specimens are shown in Figure 2(a), and roughness of the curved surface is $R_z = 2.6$ μm. Axial loading fatigue experiments were carried out at room temperature on QBG-50 high frequency fatigue testing machine, the test frequency was in the 100 HZ, and $R = 0.1$ load ratio. According to the stair-case method, at least four specimens were performed to the final failure or to the maximum life of 10^7 cycles for each data point on the S–N curve. The S–N curves of the three tempered samples were determined, and fitting curves were obtained. Heat treated tensile tests with thickness of 2.5 mm (Figure 2(b)) were performed on a MTS 810 servo hydraulic testing machine using the specimens with gauge length of 12.5 mm. The dimension of the impact specimens is 10 mm × 10 mm × 50 mm. After etching with the solution of 2% nitric acid alcohol, optical microstructure of the samples was observed on MeF3A type metallurgical microscope, and SEM images were taken on a LEO1450 secondary electron microscopy. Information on pore size and pore morphology was obtained using SEM images with magnification of 500× and image analysis technique. Twenty measurements were taken for each material.

Table 1. Chemical compositions of PM sintered low-alloy steels (wt-%).

Samples	Ni	Mo	Cu	Cr	C	Fe
0.5Cu	2	0.5	0.5	0	0.5	Bal.
1.5Cu	4	0.5	1.5	0	0.5	Bal.
0.5Cr	4	0.5	1.5	0.5	0.5	Bal.

Microscopic analyses of the impact- and fatigue-fracture surface were carried out on LEO1450 scanning electron microscopy.

Results and discussion

Microstructure characterisation

The characteristics of the pores, including the amounts of pores, shapes, size and pore spacing, are critical in determining the final dynamic properties of PM steels [13]. The density of 0.5Cu, 1.5Cu and 0.5Cr alloys are 7.52, 7.54 and 7.51 g cm^{-3}, respectively. The sintered densities of the three kinds of alloys are comparable. Figure 3 shows typical pore morphology of the 0.5Cr alloy. As described by Abdoos et al., pore closing occurs at density level of >7.3 g cm^{-3} [14,15]. Total porosity of 0.5Cu alloy is less than 5%, and isolated pores prevail. The pores are evenly distributed in the microstructure. The average pore spacing is estimated to be around 203 μm, which is much larger than that of the samples with density of 7.0 g cm^{-3} (45–50 μm) [13]. The 0.5Cu and 1.5Cu alloys have similar porosity content and pore morphology with that of the 0.5Cr alloy.

Figure 4 provides pore size and pore shape distribution values of 0.5Cr alloy. It is seen from Figure 4 (a) that the 0.5Cr alloy consists mainly of the pores below 5 μm^2 in area, which is much smaller than that of the low density alloys (30–60 μm^2) [16]. Pore shape was characterised using a shape factor f_{circle} [17]

$$f_{circle=}4\pi A/P^2 \quad (1)$$

where A is the area of the pore and P is the circumference of the pore in the measurement plane. f_{circle} provides a degree of irregularity, and the degree of irregularity increases with decreasing f_{circle} from 1. It is revealed in Figure 4(b) that the f_{circle} value of 0.5Cr alloy is in the range of 0.05–0.95, and f_{50} is around 0.57. The f_{50} values of 0.5Cu and 1.5Cu alloys are measured to be 0.47 and 0.60, respectively. The relatively regular pores of the 1.5Cu and 0.5Cr alloys is

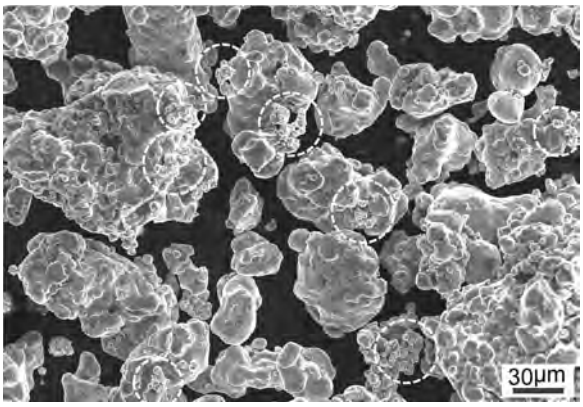

Figure 1. Typical SEM morphology of binder-treated ferrous powder mixture.

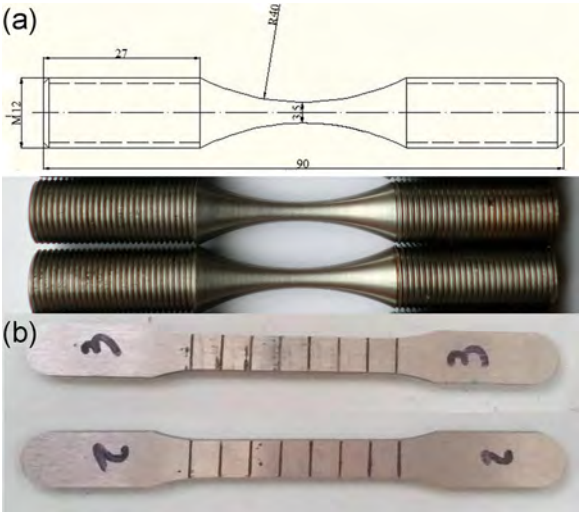

Figure 2. Geometry of the unnotched fatigue test specimens.

attributed to the increased Cu content, which promotes liquid phase sintering and the blunting of sharp edges inside the pores. This is beneficial to limit crack nucleation and improve the fatigue strength of PM steels.

In the high-density PM steels, a decrease in porosity reduces the influence of porosity on fatigue life, while microstructural effect becomes more important. Figure 5 presents optical microstructure of the three kinds of tempered PM steels. The 0.5Cu alloy has heterogeneous mixture of tempered martensite (M), relatively large residual pearlite (P), and residual Ni-rich austenite (NRA), as seen from Figure 5(a). As for the 1.5Cu alloy, the increased addition of Cu leads to the formation of larger amount and size of pearlite, as well as increased amount of retained austenite due to the increased content of Ni, as shown in Figure 5(b). The overall microstructure of the 0.5Cr alloy is more homogeneous. It comprises martensite as predominant phase, a significant amount of upper and lower bainite, some small area of pearlite, and uniformly distributed Ni-rich areas, as shown in Figure 5(c). Compared with the 1.5Cu alloys, the 0.5 wt-% Cr addition promotes the formation of Ni-rich martensite and bainite at the expense of pearlite, which is beneficial to strengthen and homogenise the microstructure [18]. At the same time, pronounced decrease of Ni-rich austenite is observed. The tempered martensite is composed of lath martensite and plate martensite, as clearly displayed in Figure 5(d).

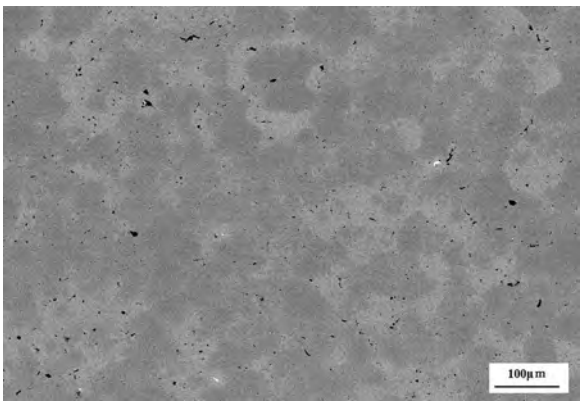

Figure 3. Typical pore morphology of 0.5Cr alloy.

Microstructure of PM steels depends on the local composition of difference areas. In the 0.5Cu alloy, pearlite is formed at the C-rich core of the original iron powder, while Ni-rich austenite is formed at the border of the powder particles. The 1.5 wt-% Cu addition results in the formation of coarse degenerate pearlite with thick cementite plate. The addition of Ni increases the chemical potential of C, and Ni diffusion is retarded by the C dissolved in steel matrix due to the strong repulsion between Ni and C, leading to the formation of Ni-rich areas [19]. After quenching, the Ni-rich areas stabilise austenite, while the remaining partially alloyed iron with less alloying elements transforms to Ni-rich martensite. The increased addition of Ni is found to result in the formation of a large amount of Ni-rich austenite and Ni-rich martensite at the expense of pearlite, which is in agreement with the result reported by Wu et al. [20]. Element Cr alleviates the strong repulsion between Ni and C, thus promoting the homogenisation of Ni. With the decreasing of Ni concentration in the sintered necks and the periphery of the original iron powder, larger area of Ni-rich martensite is formed after quenching. This heterogeneous microstructure is a kind of composite-like structure, which consists of hard phase (Ni-rich martensite) and soft phase (Ni-rich austenite).

Figure 6 displays the backscattered electron and secondary electron images of the tempered 1.5Cu and 0.5Cr alloys. Obvious Ni-rich areas are observed in 1.5Cu alloy (Figure 6(a)). As for 0.5Cr alloy, the 0.5 wt-% Cr addition contributes to the diffusion homogenisation of Ni, and the microstructure is further homogenised and strengthened (Figure 6(b)). With the further diffusion of Ni into the steel matrix, Ni-rich austenite decreases and Ni-rich martensite increases in the 0.5Cr alloy. Figure 6(c,d) shows the secondary electron images of the 1.5Cu and 0.5Cr alloys etched with nital-picral. The austenite area remains light and smooth, while martensitic steel matrix is revealed. Compared between Figure 6(c,d), it is seen that the 1.5Cu alloy has relatively large Ni-rich austenite area than that of the 0.5Cr alloy. Retained austenite is detrimental to static properties but beneficial to fatigue strength up to a certain level [21].

Tensile and impact properties

Tensile and impact behaviours of PM steels are of great technological importance for the components used under dynamic loading. Figure 7(a) shows the stress–strain curves of the three kinds of alloys. All the alloys

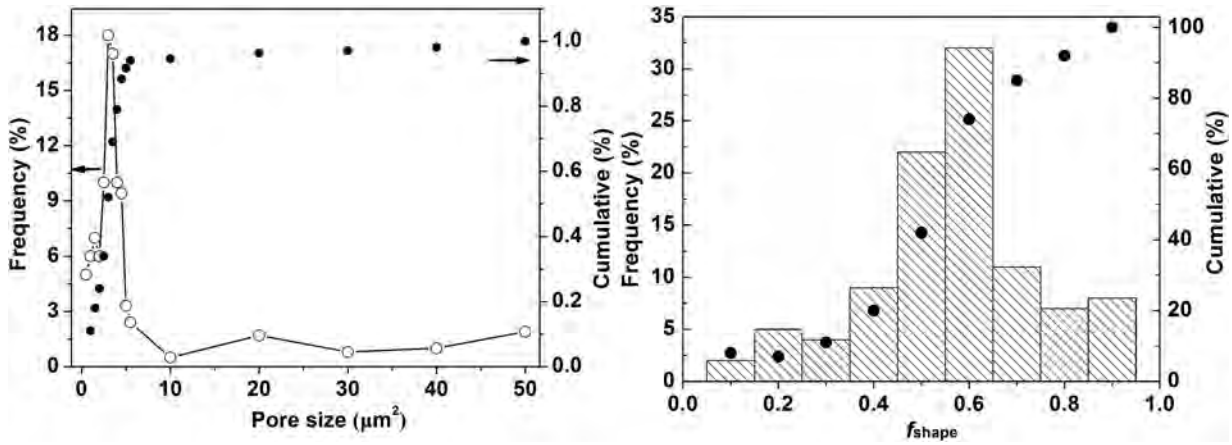

Figure 4. Pore size (a) and pore shape (f_{circle}) distribution (b) values of 0.5Cr alloy.

exhibit continuous yielding under tensile testing. During tensile loading, the localisation of plastic deformation in the weakest regions at the pore edges and the possible formation of microcracks further increase damage accumulation in the alloys, which favours the continuous yielding behaviour [22]. Table 2 lists carbon and oxygen contents and static mechanical properties of the three kinds of PM steels. The 0.5Cr alloy shows slightly higher oxygen content than that of the other two kinds of alloys due to its high affinity for oxygen, but it exerts no obvious detrimental effect on mechanical properties. The tensile strength of 0.5Cu, 1.5Cu and 0.5Cr are 1194, 1270 and 1350 MPa, respectively. The data in brackets is the standard deviation. The 0.5Cu alloy lack enough matrix hardening element copper and relatively larger residual pearlite, leading to the relatively low tensile strength. Compared with 0.5Cu alloy, the improved tensile strength of 1.5Cu alloy is attributed to the fact that copper activates sintering and improves pore size through the effect of transient liquid phase. The 0.5Cr alloy has the highest tensile strength, which is ascribed to the

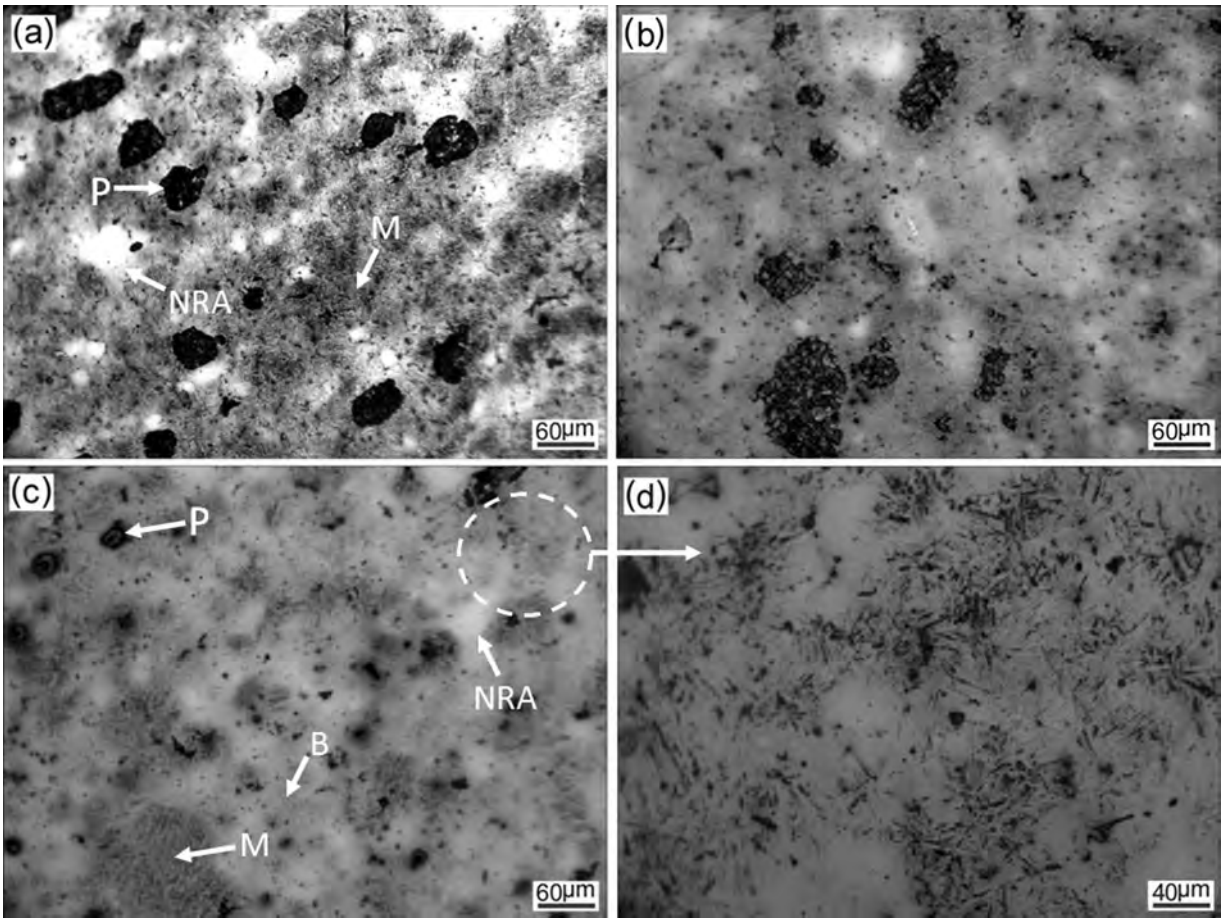

Figure 5. Optical microstructure of the three kinds of tempered PM steels: (a) 0.5Cu; (b) 1.5Cu; (c, d) 0.5Cr.

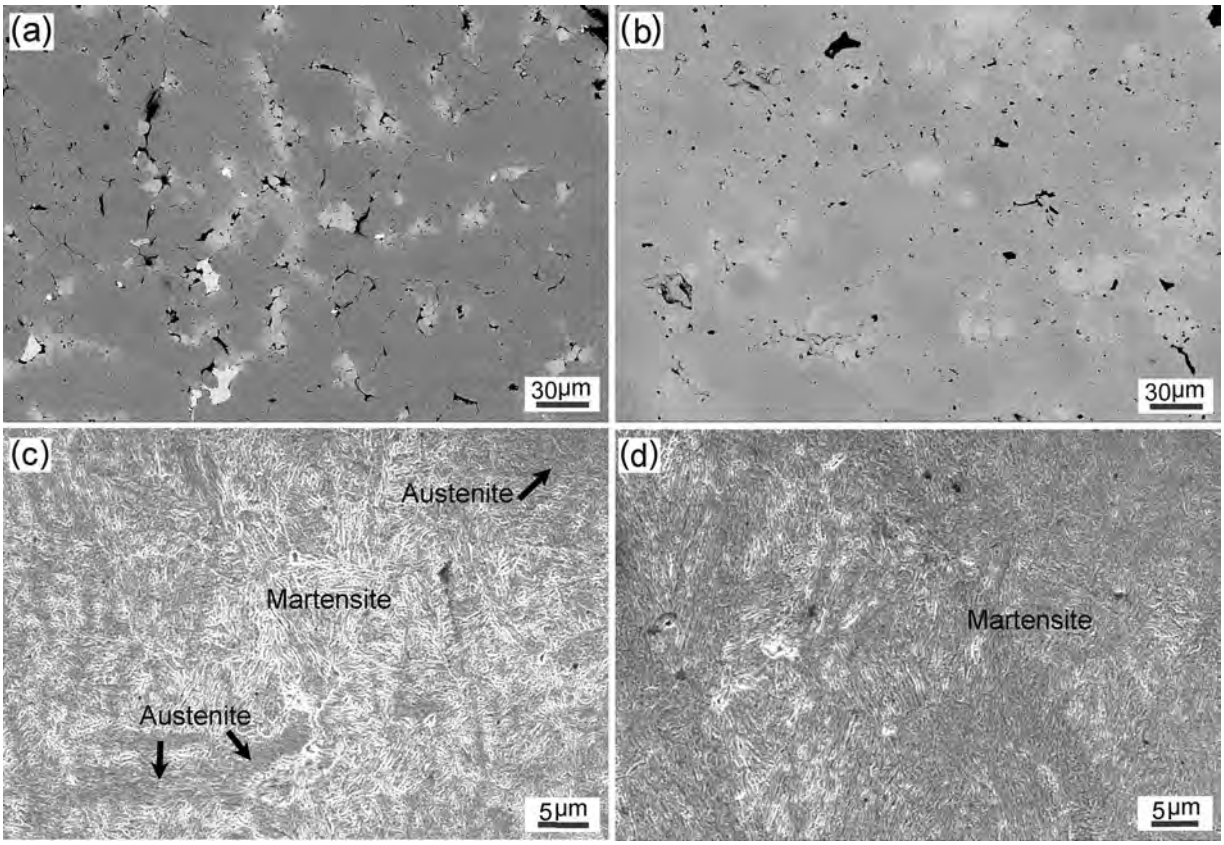

Figure 6. Backscattered electron images and secondary electron images of the tempered PM steels: (a) 1.5Cu alloy, BEI, unetched; (b) 0.5Cr alloy, BEI, unetched; (c) 1.5Cu alloy, SEI, etched; (d) 0.5Cr alloy, SEI, etched.

homogenisation of the microstructure and the formation of composite-like structure. Additionally, the ductility of 0.5Cu, 1.5Cu and 0.5Cr alloy is in the range of 2.0–2.4%. Due to the enhanced densification and diffusion of alloying elements, the matrix is hardened significantly, and the stress relaxation capacity of the matrix is reduced. Localised plastic deformation starts and the stress in the vicinity of the pores increase very rapidly, and fracture starts at relatively low average stress level. This is responsible for the low ductility of the alloy.

The impact energies of 0.5Cu, 1.5Cu and 0.5Cr are 22.9, 18.7 and 21.1 J, respectively. On the consideration of the similar porosity and pore shape of the three kinds of alloys, impact toughness of PM steels depends mainly on the microstructure. It is reported in wrought steels and PM steels that pearlite and Ni-rich austenite are not as tough as bainite and Ni-rich martensite, and they are the vulnerable sites during impact testing and must be eliminated in order to improve impact toughness of PM steels [23]. Addition of Cu to PM steel has beneficial and detrimental effects to the strength in two ways. It improves the bond between powder particles through liquid phase sintering and reduces the impact property by stabilising the softer retained austenite [24,25]. The 1.5 wt-% Cu addition results in the formation of coarse degenerate pearlite at the expense of tougher martensite and thus impaired the impact toughness of Ni-containing PM steel, though it does improve the tensile strength. The thick cementite plates could be another cause of the low toughness of 1.5Cu alloy. In the case of 0.5Cr alloy, most of the low-toughness pearlite was replaced by the strong and tough Ni-rich martensite. As a result, the 0.5Cr alloy exhibits a superior combination of tensile strength and toughness. The fine microstructural feature also contributes to its higher toughness [26]. Figure 7(b)–(d) displays the impact-fractured surfaces of the alloys. The 0.5Cu alloy displays dimpled ductile fracture along with the presence of some cleavages, as shown in Figure 7(b). Moreover, the ductile failure regions are highly localised in sinter bonds. The impact fracture surface of 1.5Cu alloy appears relatively flat and smooth, and it exhibits localised ductile failure and a higher percentage of shear fractures due to the existence of relatively large area of brittle pearlite (Figure 7(c)). Shear fractures suggest that the alloy breaks with small plastic deformation before fracturing. The 0.5Cr alloy exhibits mainly dimpled ductile fracture, and it has a larger quantity of deep, open dimples with high deformation (Figure 7(d)).

Fatigue property

In Figure 8, the stress amplitude–cycle number (S–N) plots of the three kinds of tempered PM steels are shown. It reveals that up to $N = 10^7$, there is nothing like a true 'fatigue limit', i.e. a horizontal section of

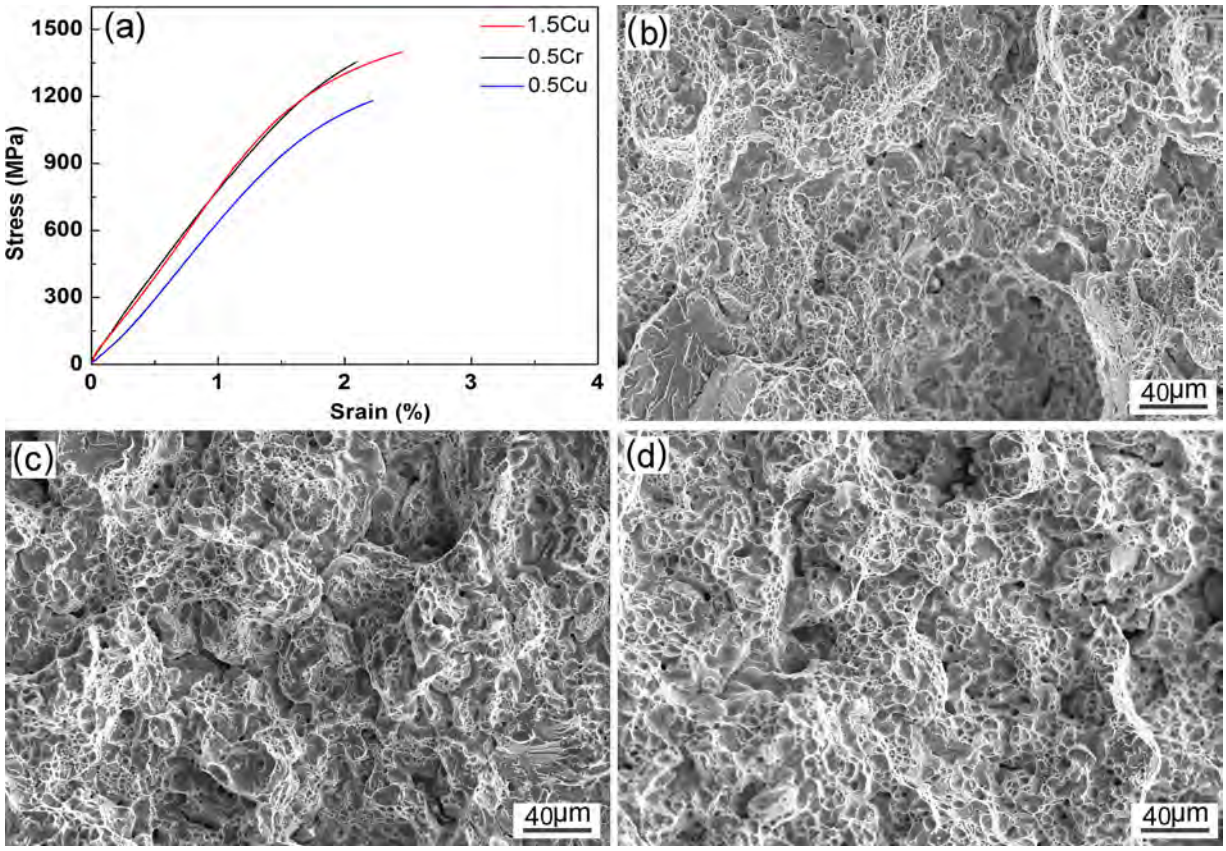

Figure 7. Stress–strain curves (a) and impact-fractured surfaces of the three kinds of PM steels: (b) 0.5Cu; (c) 1.5Cu; (d) 0.5Cr.

the S–N graph at higher N. All S–N curves consistently drop with increasing N. There is no traditional horizontal zone formed in the range of 10^6–10^7 cycles, and only the fatigue endurance strength exists. Under 10^7 cycles the fatigue endurance strength of 0.5Cu, 1.5Cu and 0.5Cr alloys are 509, 538 and 562 MPa, respectively. These values are much higher than that of the specimens with lower density, which can at least in part be attributed to the transition from interconnected to isolated pores. The local applied stress intensity factor, K_{loc}, can be calculated using the expression [17]:

$$K_{loc} = \frac{Y\sigma\sqrt{\pi a}}{\Phi} \tag{2}$$

where Y is a geometric constant that accounts for crack size and crack shape, σ is the nominal applied stress, and a is the mean pore radius. It is seen that stress intensity decreases with the decrease of crack size and the increase of geometric constant [26]. During fatigue tests, crack initiation and growth is mainly sensitive to the microstructure. The fatigue strength of 1.5Cu alloy is the lowest since the brittle pearlite in the microstructure allows for easy formation of microcracks. The existence of coarse retained pearlite consisting of high angle boundary poor region deteriorates the fatigue properties of the 0.5Cu alloy. The 0.5Cr alloy yields the highest fatigue strength, which is attributed to high sintered density, an excessive increase in the matrix strength with the homogenisation of alloying elements, rounder pores, and more favourable composite-like microstructure. The soft phase (Ni-rich austenite) in the composite-like microstructure contributes to the enhancement of fatigue strength to a certain

Table 2. The tensile strength and impact toughness of the three kinds of PM steels.

Samples	Carbon content (%)	Oxygen content (%)	Tensile strength (Mpa)	Impact energy (J cm^{-2})	Ductility
0.5Cu	0.46	0.24	1194 (35)	22.9 (1.1)	2.2%
1.5Cu	0.48	0.22	1281 (29)	18.5 (1.2)	2.0%
0.5Cr	0.43	0.30	1350 (23)	21.1 (0.9)	2.4%

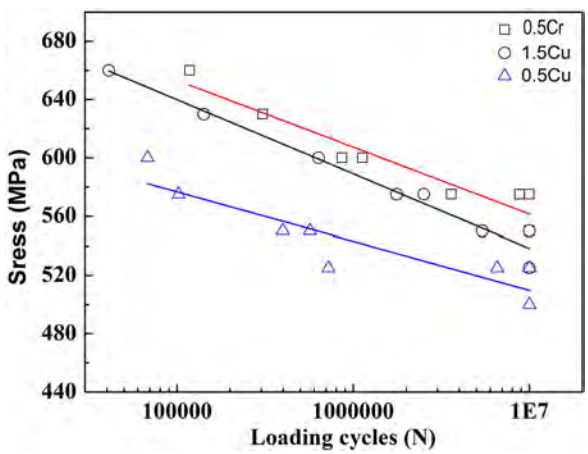

Figure 8. S–N curves of the three kinds of PM steels.

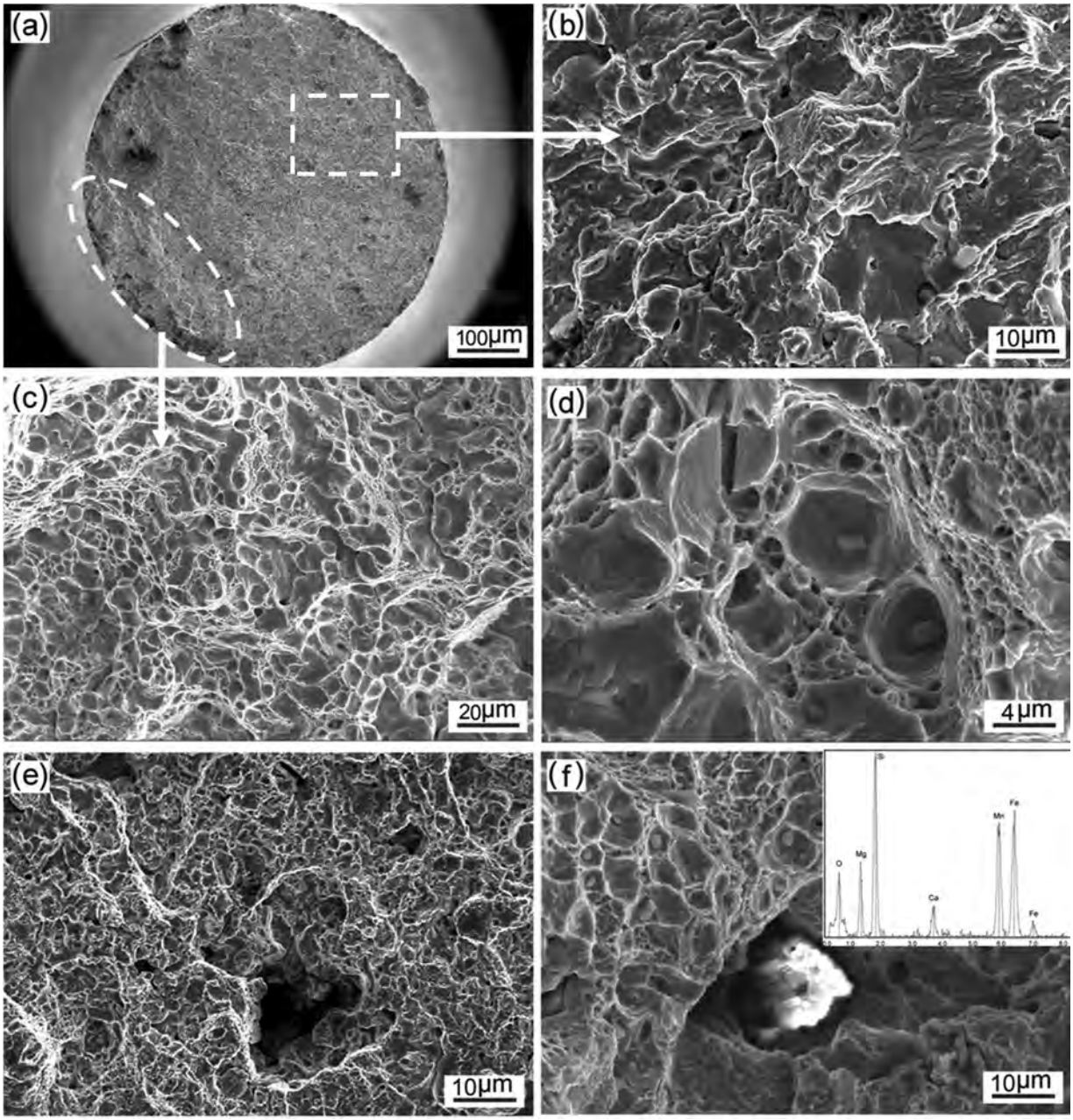

Figure 9. Fatigue-fracture morphology of the 0.5Cu alloys under the load of 500 MPa.

extent. Some retained austenite is transformed to martensite during cyclic loading, thus increasing fracture resistance [22]. Additionally, when a crack encounters a region of soft retained austenite, it is diverted and branched or blunted.

Fatigue-fracture morphology was investigated in order to reveal the fatigue-fracture mechanism of the alloys. Figure 9 shows fatigue-fracture morphology of 0.5Cu alloys under the load of 500 MPa. A relatively small crack origin area (marked by the circle) and a large instant rupture area were observed in Figure 9 (a). The instant rupture area is relatively smooth, and it consists of mainly transgranular fracture, cleavage planes, pits and tearing edges, as revealed in Figure 9 (b). The crack origin area is characterised by rough morphology, and numerous micro voids and equiaxed dimples appear in the crack origin area (Figure 9(c)), indicating severe plastic deformation occurred in local fracture zone. Cleavage crossing the brittle area is observed in Figure 9(d). The cleavage crossing the pearlite and the ductile fracture at the sintered necks were the primary causes of the fracture. The secondary crack originated in the internal pores or non-metallic inclusions interior of the specimen (Figure 9(e)). Interlinking of cracks is not observed due to the large pore spacing. Figure 9(f) shows that the inclusions occur in the crack propagation, which are mainly oxides and sulphides with constituents of O, Si and Mn.

Figure 10 shows fatigue-fracture morphology of the 1.5Cu alloy under the load of 525 MPa. The 1.5Cu alloy demonstrates comparable fracture modes with that of the 0.5Cu alloy. The difference lies in that the crack

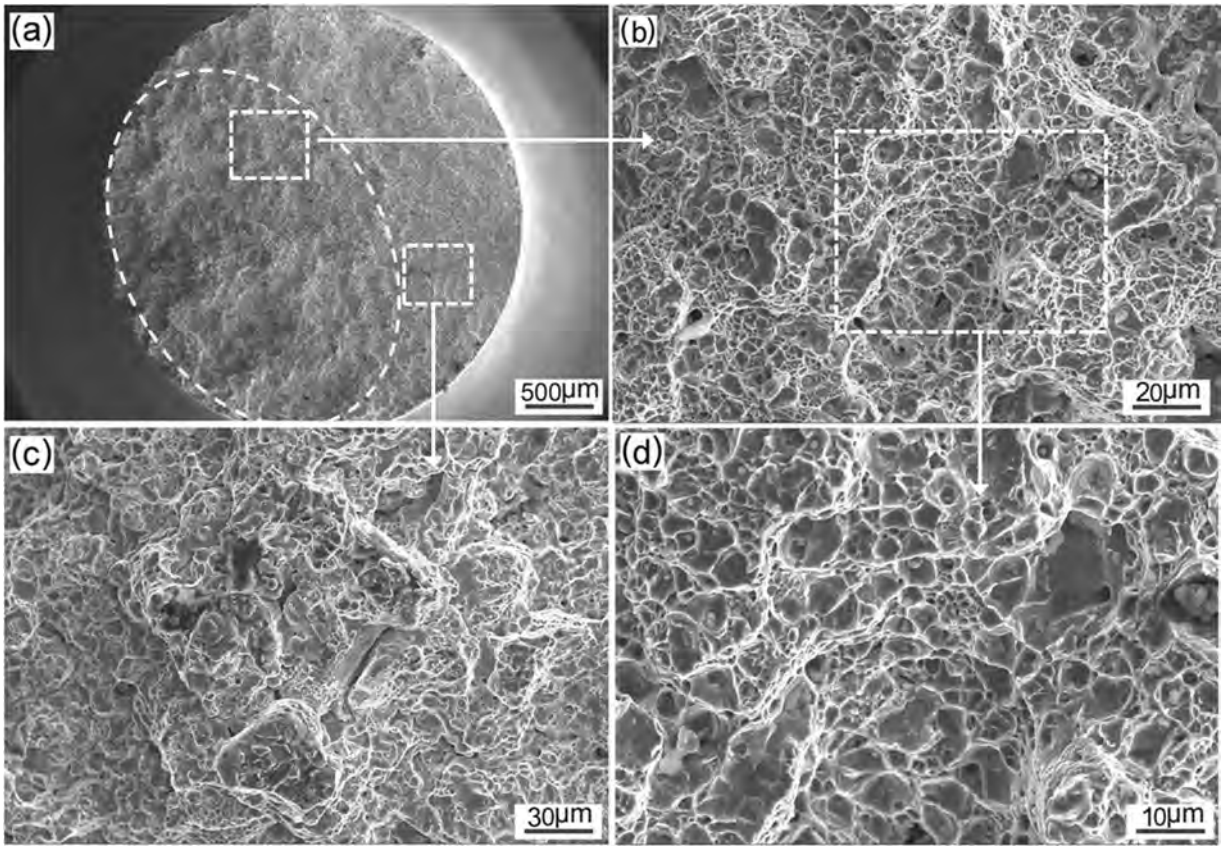

Figure 10. Fatigue-fracture morphology of the 1.5Cu alloys under the load of 525 MPa.

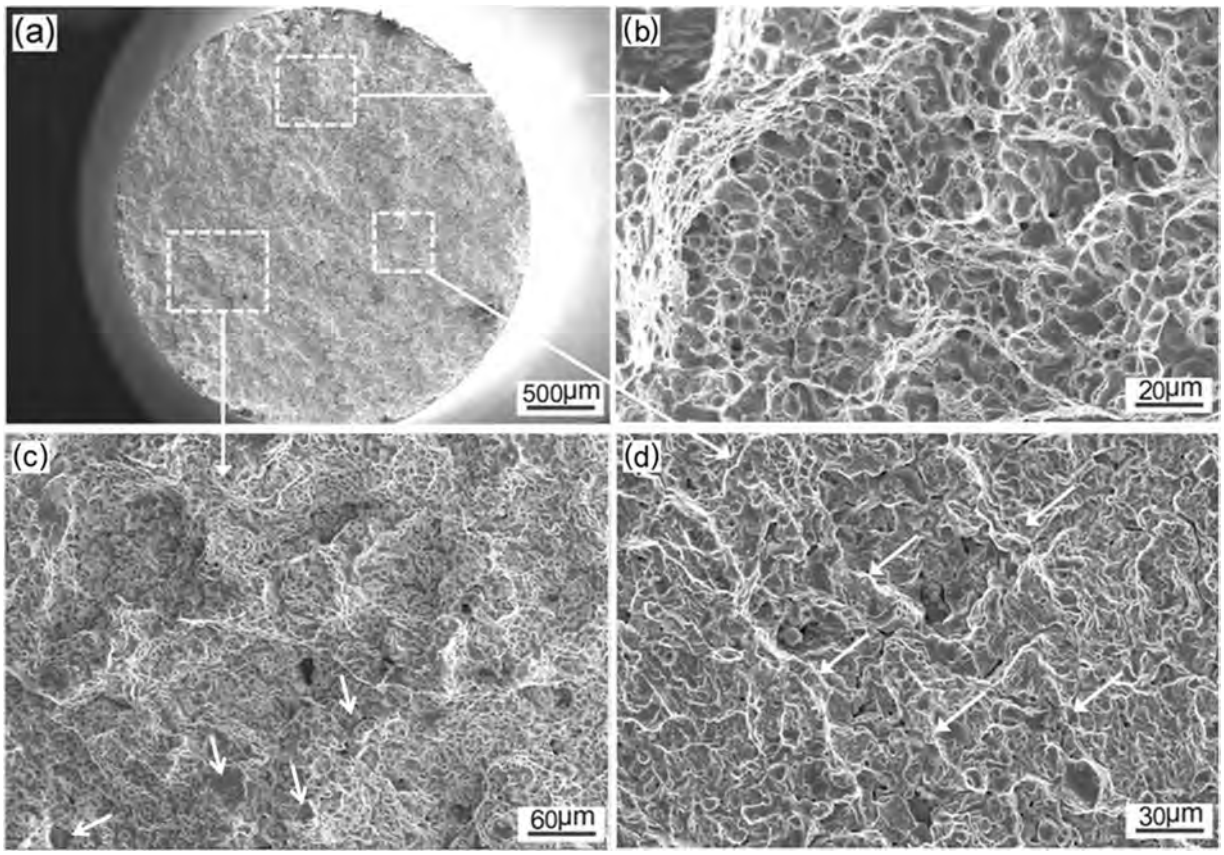

Figure 11. Fatigue-fracture morphology of the 0.5Cr alloys under the load of 550 MPa.

origin area (marked by the circle) is much larger than that in the 0.5Cu alloy, while the instant rupture area is much smaller, as shown in Figure 10(a). It is known that the fatigue cracks tend to initiate near pores or pore clusters because of the high localised stress intensity [27]. However, the 1.5Cu alloy shows the origin of the fatigue crack located interior of the specimen, and there are no clearly identifiable defects that have caused cracking. It is possible that crack nucleated independently at several sites [28]. Compared with Figure 9(b,c), the proportion of dimples decreases, the number of cleavage facets decreases, and fatigue striations appears in 1.5Cu alloy, as displayed in Figure 10(b,c). Striation occurs when plastic strains at the crack tip causes localised slip on the planes of maximum shear, and crack front undergoes repetitive blunting and sharpening during propagation during cyclic loading [29]. Some small unevenly distributed fatigue striations are observed in Figure 10 (d). This is ascribed to the multiple sites of favourable orientation and size [22].

Figure 11 presents fatigue-fracture morphology of the 0.5Cr alloy under the load of 550 MPa. The fracture surface exhibits rough morphology (Figure 11(a)). Typical morphology, such as dimples (Figure 11(b)), cleavage facets (marked by the arrows in Figure 11(c) and fatigue striations (Figure 11(d)), appeared on the fracture surface. The grid of dimple is clearly observed at high magnification in Figure 11(b). Fatigue striations are observed clearly in Figure 11(d). It is seen that there is no obvious variation in the distance between striations and the length of each striation steps, suggesting stable crack growth during fatigue-crack propagation. In the high-density alloy, microstructure heterogeneities contribute to a decrease in stress intensity at the pores and increase the number of cycles to fatigue-crack initiation. The soft Ni-rich austenite at the crack tip seems to retard fatigue-crack growth by blunting caused by plastic deformation at the tip of the microcracks. The 0.5Cr alloy has a good potential for resistance against fatigue-crack propagation.

Conclusion

The effect of alloying elements and microstructure and dynamic performance of high-density (7.5 g cm^{-3}) low-alloy PM steels were studied, and the following results are summarised:

(1) The addition of 1.5 wt-% Cu impairs the toughness of Ni-containing PM steels by the formation of low-toughness pearlite although it improves the tensile strength. The 0.5 wt-% Cr addition promotes the formation of Ni-rich martensite and bainite at the expense of pearlite, which is beneficial to strengthen and homogenise the microstructure.

(2) A good combination of tensile strength, impact toughness and fatigue properties is achieved for 0.5Cr alloy. The tensile strength and impact energy of 0.5Cr alloy reaches 1350 MPa and 21.1 J. The fatigue endurance strength of 0.5Cr alloy achieves 562 MPa under 10^7 cycles. The enhanced fatigue life of high-density alloy is attributed to the high density, strengthened sintering necks, smaller pore size, rounder pores and composite-like microstructure, which significantly delay the initiation of fatigue crack.

Funding

This work is financially supported by National Natural Science Foundation of China (51574030, 51574029, 51374027).

Notes on contributors

Lin Zhang is a Ph.D. in Materials Science and Engineering. Presently, he is working as an associate professor at the Institute for Advanced Materials and Technology of University of Science and Technology Beijing in China. His research interest includes high performance iron based alloy and oxide dispersion strengthened alloys.

Zhiwei Liu is a doctoral candidate in the Department of Materials Science and Engineering of University of Science and Technology Beijing in China. His research interest is PM iron based alloy with high density.

Haishen Sun is a doctoral candidate in the Department of Materials Science and Engineering of University of Science and Technology Beijing in China. His research interest is also PM iron based alloy with high density.

Mingli Qin is a Ph.D. in Materials Science and Engineering. Presently, he is working as a professor at the Institute for Advanced Materials and Technology of University of Science and Technology Beijing in China. His research interest includes injection molding technology and advanced MIMed materials.

Xuanhui Qu is a Ph.D. in Materials Science and Engineering. Presently, he is the dean at the Institute for Advanced Materials and Technology of University of Science and Technology Beijing in China. His research interest includes advanced powder metallurgy materials and technologies.

Yuanzhi Lyu is a B.S. He is a researcher of Laiwu Xinyi Powder Metallurgy Products Co. Ltd, Shandong, China.

References

[1] Chawla N, Polasik S, Narasimhan KS, et al. Fatigue behavior of binder-treated P/M steels. Int J Powder Metal. 2001;37(3):49–57.

[2] Beiss P, Dalgic M. Structure property relationships in porous sintered steels. Mater Chem Phy. 2013;67(1–3):37–42.

[3] Williams JJ, Deng X, Chawla N. Effect of residual surface stress on the fatigue behavior of a low-alloy powder metallurgy steel. Inter J Fatigue. 2007;29(9–11):1978–1984.

[4] Bengtsson S. Influence of density and microstructure on fatigue properties of warm compacted Fe-Cu-Ni-Mo steels. Adv Powder Metall Part Mater. 2000;6:69.
[5] Gerosa R, Rivolta B, Tavasci A, et al. Crack initiation and propagation in chromium pre-alloyed PM-steel under cyclic loading. Eng Fract Mech. 2008;75(3–4):750–759.
[6] Verdu C, Carabajar S, Lormand G. Fatigue crack growth characterization and simulation of a porous steel. Mater Sci Eng A. 2001;319–321:544–549.
[7] Polasik SJ, Williams JJ, Chawla N. Fatigue crack initiation and propagation of binder-treated powder metallurgy steels. Metall Mater Trans A. 2002;33(1):73–81.
[8] Sudhakar KV. Fatigue behavior of a high density powder metallurgy steel. Inter J Fatigue. 2000;22(9):729–734.
[9] Hadrboletz A, Weiss B. Fatigue behaviour of iron based sintered material: a review. Int Mater Rev. 1997;42:1–44.
[10] Khorsand H, Habibi SM, Jonghorban K, et al. Fatigue of sintered steels. Mater Struct. 2004;37:335.
[11] Carabajar S, Verdu C, Hamel A, et al. Fatigue behaviour of a nickel alloyed sintered steel. Mater Sci Eng A. 1998;257:225–234.
[12] Prasad SN, Mediratta SR, Sarma DS. Influence of austenitisation temperature on the structure and properties of weather resistant steels. Mater Sci Eng A. 2003;358:288–297.
[13] Chawla N, Murphy TF, Narasimhan KS, et al. Axial fatigue behavior of binder-treated versus diffusion alloyed powder metallurgy steels. Mater Sci Eng A. 2001;308:180–188.
[14] Abdoos H, Khorsand H, Shahani AR, et al. The effect of microstructure heterogeneity on fatigue property of powder metallurgy steels. Defect Diffusion Forum. 2008;273–276:348–353.
[15] Dlapka M, Danninger H, Gierl C, et al. Defining the pores in PM components. Metal Powder Report. 2010;65:30–33.
[16] Cipolloni G, Menapace C, Cristofolini I, et al. A quantitative characterisation of porosity in a Cr-Mo sintered steel using image analysis. Mater Charact. 2014;94:58–68.
[17] Straffelini G, Fontanari V, Hafez A, et al. Tensile and fatigue behaviour of sinter hardened Fe–1·5Mo–2Cu–0·6C steels. Powder Metall. 2009;52:298–303.
[18] Wu M-W, Tsao L-C, Chang S-Y. The influences of chromium addition and quenching treatment on the mechanical properties and fracture behaviors of diffusion-alloyed powder metal steels. Mater Sci Eng A. 2013;565:196–202.
[19] Shanmugasundaram D, Chandramouli R. Tensile and impact behaviour of sinter-forged Cr, Ni and Mo alloyed powder metallurgy steels. Mater Design. 2009;30:3444–3449.
[20] Wu MW, Tsao LC, Shu GJ, et al. The effects of alloying elements and microstructure on the impact toughness of powder metal steels. Mater Sci Eng A. 2012;538:135–144.
[21] Lu Y-H, Xiao Z-Y, Hu L, et al. Ultra-high cycle fatigue behaviour of warm compaction Fe-Cu-Ni-Mo-C sintered material. Mater Design. 2014;55:758–763.
[22] Straffelini G, Benedetti M, Fontanari V. Damage evolution in sinter-hardening powder-metallurgy steels during tensile and fatigue loading. Mater Design. 2014;61:101–108.
[23] Straffelini G, Menapace C, Molinari A. Interpretation of effect of matrix hardening on tensile and impact strength of sintered steels. Powder Metall. 2002;45:167–172.
[24] Wong-ángel WD, Téllez-Jurado L, Chávez-Alcalá JF, et al. Effect of copper on the mechanical properties of alloys formed by powder metallurgy. Mater Design. 2014;58:12–18.
[25] Mellanby IJ, Moon JR. Fatigue properties of heat-treatable low alloy powder metallurgy steels. Metal Powder Report. 1989;44:432–435.
[26] Bernier F, Plamondon P, Baïlon J-P, et al. Microstructural characterisation of nickel rich areas and their influence on endurance limit of sintered steel. Powder Metall. 2011;54:559–565.
[27] Abdoos H, Khorsand H, Shahani AR. Fatigue behavior of diffusion bonded powder metallurgy steel with heterogeneous microstructure. Mater Design. 2009;30:1026–1031.
[28] Gerard DA, Koss DA. The influence of porosity on short fatigue crack growth at large strain amplitudes. Int J Fatigue. 1991;13:345–352.
[29] Danninger H, Xu C, Khatibi G, et al. Gigacycle fatigue of ultra high density sintered alloy steels. Powder Metall. 2012;55:378–387.